Vol. 89: 99–117, 2023
https://doi.org/10.3354/ame01999

AQUATIC MICROBIAL ECOLOGY
Aquat Microb Ecol

Published August 3

Biological mechanisms underlying priming of vascular plant material in the presence of diatoms

Patricia Bonin[1,*], Aurélie Portas[1], Julie Hardy[1], Sophie Guasco[1], Thomas S. Bianchi[2], Nicolas D. Ward[3,4], Jean-François Rontani[1]

[1]Aix Marseille Univ, Université de Toulon, CNRS, IRD, MIO UM 110, 13288 Marseille, France
[2]Department of Geological Sciences, Box 112120, University of Florida, Gainesville, FL 32611-2120, USA
[3]Marine and Coastal Research Laboratory, Pacific Northwest National Laboratory, 1529 W Sequim Bay Rd, Sequim, WA 98382, USA
[4]School of Oceanography, University of Washington, Box 355351, Seattle, WA 98195, USA

ABSTRACT: Priming effects that stimulate increased degradation of refractory organic matter by microorganisms following fresh organic matter input is a well-known phenomenon in terrestrial environments but remains controversial in marine environments. We used a combination of chemical (gas chromatography-EI quadrupole time of flight mass spectrometry) and molecular biology (DNA stable-isotope probing [DNA-SIP]) methods to trace the fate of terrestrially derived particulate organic matter (TPOM) and the response of the marine microbial community to fresh organic matter inputs. We tested the potential for priming effects among a mixture of marine and terrestrial microbial assemblages, amended either with only ^{13}C-labelled TPOM (^{13}C-*Avena sativa*) or with an addition of ^{12}C-*Skeletonema costatum* (a marine diatom) as a labile co-substrate within the range of diatom concentrations found in estuaries. We monitored ^{13}C-labelled TPOM lipid tracers (long-chain fatty acids, *n*-alkan-1-ols, phytol, sitosterol, β-amyrin and components of cutins) throughout a 42 d incubation experiment. Comparisons with controls carried out without diatom addition showed faster decay of phytol, *n*-alkan-1-ols, and components of cuticular waxes in the presence of diatoms, while fatty acids and sitosterol were unaffected. Bacteria belonging to the *Bacteroidota* phylum (mainly *Flavobacteria* and *Cytophaga*) were the dominant microbes involved in priming-induced TPOM degradation in the incubation treatments. *Sphingomonadales* and *Rhizobiales*, capable of lignin and hemicellulose degradation, also contributed to the degradation of TPOM but did not seem to contribute to priming effects related to increased diatom abundance. These lab-based results demonstrate direct evidence that priming of TPOM occurred selectively via a consortium of microbes.

KEY WORDS: Priming effect · Bacteria · DNA-SIP analyses · ^{13}C-labelling · *Avena sativa* · *Skeletonema costatum* · Rhône suspended particulate matter (SPM) · Lipids

Resale or republication not permitted without written consent of the publisher

1. INTRODUCTION

Rivers export substantial amounts of terrestrially derived particulate organic matter (TPOM) to the coastal ocean (e.g. Berner 1982, Hedges et al. 1997). However, there remain critical gaps in our understanding of the behavior of this material along the river-ocean continuum (e.g. Ward et al. 2017). Organic molecules associated with higher plants such as lignocellulose have historically been considered recalcitrant to marine microbial decay pathways (de Leeuw & Largeau 1993, Hedges 2002, Bianchi et al.

*Corresponding author: patricia.bonin@mio.osupytheas.fr

© Inter-Research 2023 · www.int-res.com

2013). Interestingly, early work also showed that coastal marine sediments stored less TPOM than predicted from global river inputs (Hedges & Keil 1995). This implied that TPOM global budgets were either incorrect or that TPOM experienced greater degradation than expected in coastal waters, and/or was exported to offshore waters more than expected (Hedges et al. 1997, Burdige 2005, Bianchi 2011). More recently, this paradigm has changed showing that TPOM can, in fact, be substantially decomposed by microbes in coastal waters (e.g. Vonk et al. 2010, Bourgeois et al. 2011, Karlsson et al. 2011, Rontani et al. 2014, Bianchi et al. 2018). However, the diversity of microorganisms responsible for TPOM decay (Pointing & Hyde 2000, Björdal 2012) and their relative role in pre- and post-depositional processes that control TPOM stocks in the coastal ocean remain largely unexplained.

Coastal TPOM degradation is likely carried out by a microbial consortium with different metabolic functions and enzymes. The dynamic nature of the coastal zone can result in complex relationships whereby TPOM-degrading microbial distribution patterns are not actually linked with TPOM concentration gradients. For example, *Gammaproteobacteria*, which are abundant in TPOM-depleted saline waters, were found to be more efficient at degrading TPOM than *Betaproteobacteria*, which dominate TPOM-rich river waters (Newton et al. 2011, Bonin et al. 2019). The decay of TPOM may also be enhanced by unique interactions between different metabolic pathways across steep physicochemical gradients, or aquatic critical zones (Bianchi & Morrison 2018), where turbid nutrient-rich river waters interface with phytoplankton-rich marine waters. Finally, although marine fungi (e.g. *Ascomycetes*) have long been recognized for their capability of decomposing TPOM in coastal waters (Jones & Irvine 1971, Benner et al. 1984, Mouzouras 1989), they have largely been ignored in coastal carbon cycling, but with some recent renewed interests (Pointing & Hyde, 2000, Blanchette 2010, Björdal & Dayton 2020).

The term 'priming effect' more broadly describes a suite of interactive microbial processes (e.g. Bengtsson et al. 2018). While well-studied and demonstrated in soils (Parnas 1976, Kuzyakov et al. 2000, Bastida et al. 2019), priming effects are less constrained in aquatic systems and are generally described as an enhanced remineralization of terrestrially derived material in the presence of labile cosubstrates from algal sources (e.g. Bianchi et al. 2011, 2015, Guenet et al. 2014, 2018, Steen et al. 2016, Aller & Cochran 2019, Ward et al. 2019a,b). Inconsistencies in the detection of priming in aquatic systems may, in part, be related to the diversity of indices used to 'track' priming (e.g. change in CO_2, nutrient production/uptake, bacterial production, enzyme assays, loss of primed substrate) and/or where the work was conducted (e.g. field or laboratory) (Sanches et al. 2021). Nevertheless, priming of recalcitrant organic matter (OM) in aquatic systems is generally hypothesized to result from (1) an increase of microbial biomass due to consumption of reactive substrates (algal components) (Grant & Betts 2004), or (2) an enhanced microbial production of extracellular enzymes capable of breaking down less reactive substrates (TPOM components), driven by energy obtained from the breakdown of more reactive substrates (e.g. amino acids and simple sugars) (e.g. Ward et al. 2016, Guenet et al. 2018). Coastal deltaic regions, characterized by a high input of TPOM, high rates of primary production, and high respiration rates via microbial communities, are generally considered to have a high priming potential (Bianchi 2011, Guenet et al. 2018). Unfortunately, the specific mechanistic pathways involved in the degradation of primed TPOM in aquatic systems remains poorly understood (Bengtsson et al. 2018, Sanches et al. 2021). Such knowledge may be critical for accurately portraying how coastal biogeochemical dynamics influence carbon fluxes and nutrient cycling in the context of global climate changes (Ward et al. 2020, Bianchi et al. 2021).

A recent experiment observed enhanced TPOM degradation of suspended particulate matter (SPM) in the Rhône River after a phytoplankton bloom dominated by diatoms based on specific lipid tracer analyses (amyrins, lupeol, phenolic acids, and components of cuticular waxes) (Bonin et al. 2019). This enhanced TPOM biodegradation might be attributed to the presence of diatoms; however, due to the use of distinct SPM inocula during these experiments this enhancement may have also resulted from the presence of a more efficient bacterial community during the bloom period (Bonin et al. 2019). Thus, the role of priming effects on TPOM degradation in this ecosystem could not be unequivocally demonstrated. Building on this previous work, ^{13}C-labelled *Avena sativa* ('common' oat, a C_3 grass — widespread throughout the Rhône River; Lecornu & Michel 1986) was incubated in the dark in natural seawater, in the presence and absence of the marine diatom *Skeletonema costatum,* supplemented with SPM collected in the Rhône River. The seawater and SPM served as marine and terrestrial bacterial inoculum, respectively. Quantification of labelled lipid tracers allowed us to

better track the priming of river-borne TPOM remineralization in the presence of marine diatom material. Measurement of ^{13}C-incorporation in bacterial and fungal fatty acids, along with DNA stable-isotope probing (DNA-SIP) analyses, allowed for the identification of the dominant microbes involved in the enhanced degradation of TPOM to test the hypothesis that priming-induced TPOM degradation involves a diversity of microbial actors.

2. MATERIALS AND METHODS

2.1. Sample collection

Fresh SPM samples were collected using a Teflon-coated high-speed centrifuge (CEPA Z61) at the Arles station of the MOOSE program (43° 40′ 44″ N, 4° 37′ 16″ E) (at 30 km upstream of the Rhône River mouth) on 17 December 2018. SPM samples were transported in an ice box to the laboratory and then stored at 4°C until further analysis. Seawater samples, for lab incubations, were collected on 7 December 2018 at the station SOLEMIO (SOMLIT network) (43° 14′ 30″ N, 5° 17′ 30″ E) (in the Gulf of Marseille) and filtered through GF/F (0.8 µm) before use. At the time of sampling, the salinity was 38 g kg^{-1} (measured using an ATAGO ATC refractometer).

2.2. Substrate

^{13}C-abelled (97% ^{13}C) leaves of *Avena sativa* were obtained from IsoLife. Leaves were cut into small pieces and then ground in a Fast Prep-24^{TM} 5G (MP Biomedicals), using metal beads (2 mm diameter).

2.3. Biodegradation experiments

Incubation experiments were performed in a growth chamber at a controlled temperature of 15°C — the temperature of ambient coastal waters at the time of sampling. Experimental systems were composed of 10 mg of ^{13}C labelled axenic *A. sativa*, 650 µl of a culture of *Skeletonema costatum* containing 1.1×10^6 cells ml^{-1}, 150 mg of fresh SPM collected at the Arles station and 150 ml of seawater. The diatom concentrations used here (4.8×10^3 cells ml^{-1}) corresponded to the range of nanophytoplankton in the Rhône Estuary (from 2×10^3 to 3×10^4 cells ml^{-1}) (Obernosterer et al. 2005). To maintain aerobic conditions, Erlenmeyer flasks, coated with cotton plugs, were incubated in the dark on a reciprocal shaker (96 rpm, 5 cm amplitude). At each sampling times (0, 7, 15, 28 and 42 d), 3 flasks (triplicates) were sampled for lipid analyses and 3 for SIP analyses. Control flasks without diatoms were also carried out in triplicate and incubated for 14 and 42 d. All samples were filtered on pre-combusted GF/F filters (Whatman) for chemical analyses and on 0.2 µm Nuclepore filters (Whatman) for SIP analyses and stored at –20°C until further analysis. Chemical analyses were only carried out on the controls incubated for 42 d.

2.4. Lipid analyses

For lipid analysis, thawed filters were placed in methanol (20 ml) with excess $NaBH_4$ (70 mg; 30 min at 20°C). This process was conducted to reduce any hydroperoxides in samples (Galeron et al. 2015), which are known to induce autoxidative damage of some lipids during the hot saponification step. After $NaBH_4$ reduction, 20 ml of water and 2.8 g KOH were added and directly saponified by refluxing (75°C) for 2 h. After cooling, samples were acidified with HCl (pH 1) and extracted (3×) with dichloromethane (DCM). The combined DCM extracts were dried over anhydrous Na_2SO_4, filtered, and concentrated by rotary evaporation at 40°C to isolate the total lipid extract (TLE).

TLEs were taken up in 300 µl of a mixture of pyridine and N,O-bis(trimethysilyl)trifluoroacetamide (BSTFA; Supelco) (2:1, v:v) and silylated for 1 h at 50°C to convert OH-containing compounds to their trimethylsilyl (TMS)-ether derivatives. After evaporation to dryness under a stream of N_2, derivatized residues were taken up in a mixture of ethyl acetate and BSTFA (to avoid desilylation of fatty acids) for analysis using gas chromatography-EI quadrupole time of flight mass spectrometry (GC-QTOF).

Accurate mass measurements were carried out in full scan mode using an Agilent 7890B/7200 GC/QTOF System (Agilent Technologies) and a cross-linked 5% phenyl-methylpolysiloxane (Macherey-Nagel; OPTIMA-5MS Accent) (30 m × 0.25 mm, 0.25 µm film thickness) capillary column. Analyses were performed in pulsed splitless mode set at 270°C, where oven temperature was ramped from 70°C to 130°C at 20°C min^{-1} and then to 300°C at 5°C min^{-1}. The pressure of the carrier gas (He) was maintained at 0.69×10^5 Pa until the end of the temperature program. Instrument temperatures were 300°C for the transfer line and 230°C for the ion source; nitrogen (1.5 ml min^{-1}) was used as a collision gas. Accurate

mass spectra were recorded across the range *m/z* 50–700 at 4 GHz with the collision gas opened. The QTOF-MS instrument provided a typical resolution ranging from 8009 to 12252 from *m/z* 68.9955 to 501.9706. Perfluorotributylamine (PFTBA) was used for daily MS calibration. Compounds were identified by comparing their time-of-flight (TOF) mass spectra, accurate masses and retention times with those of ^{12}C standards. Quantification of each compound involved extraction of specific accurate fragment ions, peak integration and determination of individual response factors using external standards and Mass Hunter software (Agilent Technologies). High resolution accurate mass full scans, obtained from GC-QTOF analyses, allowed for estimation of isotopic enrichment states of all lipids measured (Triebl & Wenk 2018).

^{13}C-labelled lipids were quantified using GC-QTOF with external ^{12}C-standards. Sitosterol, nonadecanoic acid, hexacosan-1-ol and phytol, were obtained from Sigma-Aldrich. Fatty acids and *n*-alkan-1-ols, were quantified with standards of nonadecanoic acid and hexacosan-1-ol, respectively. It is well-known that epoxides undergo alcoholysis to methoxyhydrins, hydrolysis to diols during alkaline hydrolysis, and are converted to chlorohydrins during acidification with HCl (Marchand & Rontani 2001). The degradation products of 9,10-epoxy-18-hydroxyoctadecanoic acid thus formed and 9,16- and 10,16-dihydroxyhexadecanoic acids were quantified with a standard mixture of 9- and 10-hydroxyoctadecanoic acids produced from oleic acid in 3 steps: (1) photosensitized oxidation of oleic acid in pyridine in the presence of hematoporphyrin as sensitizer, (2) $NaBH_4$-reduction of the resulting allylic hydroperoxyacids, and (3) hydrogenation of the double bond in methanol with Pd/C as catalyst.

2.5. DNA-SIP analyses

DNA stable isotope probing and metabarcoding sequencing were used to assess what bacteria were involved in ^{13}C-*A. sativa* degradation in the presence of ^{12}C-*S. costatum* as a co-substrate. After the growth of microorganisms in the presence of the substrate (^{13}C-*A. sativa*) and co-substrate (^{12}C-*S. costatum*), ^{13}C-DNA was separated from ^{12}C-DNA by isopycnic density gradient centrifugation in CsCl gradients. Within the gradient from lightest to heaviest DNA, microorganisms that consume only ^{12}C-*S. costatum,* then both ^{12}C-*S. costatum* and ^{13}C-*A. sativa* and finally only ^{13}C-*A. sativa* were explored. SIP analyses were carried out on the samples collected after 0, 7, 14, 28 and 42 d of incubation in the presence of ^{12}C-*S. costatum* and after 14 and 42 d of incubation without ^{12}C-*S. costatum*.

For each stop time, samples (individual vials) were filtered on 0.22 µm sterile filters and stored frozen at −80°C until further analysis. Each filter was treated with TE-Lysis buffer (20 mM Tris, 25 mM EDTA, 1 µg ml^{-1} Lysozyme) followed by 1% sodium dodecyl sulfate treatment. Extractions were performed twice with an equal volume of phenol-chloroform-isoamyl alcohol (25:24:1, v:v:v) pH 8, followed by a treatment with chloroform-isoamyl alcohol (24:1, v/v), DNA precipitation by isopropanol and resuspension in 50 µl of molecular biology grade water. Extracted DNA was quantified using the Qubit double-stranded DNA (dsDNA) high-sensitivity assay kit and a Qubit 2.0 fluorometer (Invitrogen).

The ^{13}C-DNA was separated from community ^{12}C-DNA by CsCl gradient centrifugation in the presence of EtBr (Lueders et al. 2004, Neufeld et al. 2007). To separate DNA by density, 10 µg of DNA was added to approximately 5.4 ml of a saturated CsCl and gradient buffer (100 mM Tris-HCl, 100 mM, KCl 0.1 M, EDTA 1 mM) and 110 µl of a stock solution 10 mg ml^{-1} EtBr in a 5.5 ml OptiSeal ultracentrifuge tube (Beckman Coulter). The final density of the solution was 1.725 g ml^{-1}. The samples were spun in an Optima XPN ultracentrifuge (Beckman Coulter) using a Beckman ntv-90 rotor at 127 000 × *g* for 40 h at 20°C. After centrifugation, gradients of density-separated DNAs were fractionated, and 10 fractions (ca. 500 µl) were collected per tube and weighed on a digital balance (precision 10^{-4} g) to confirm gradient formation. EtBr was removed by 3 successive washings with TE (10 mM Tris-HCl, 1 mM EDTA, pH 8)-butanol (50:50, v/v). The distribution of DNA in CsCl gradients was quantified by spectrophotometry (BioSpec-nano, Shimadzu). Five fractions of DNA were obtained from the heaviest (E) to the lightest (A) with band densities (BDs) of ~1.755–1.740, 1.740–1.730, 1.730–1.720, 1.720–1.710 and 1.710–1.700 g ml^{-1}. DNA was precipitated with 800 µl polyethylene glycol 6000 (1.6 M) overnight at room temperature, recovered by centrifugation 45 min at 13 000 × *g*, washed once with 500 µl 70% (v/v) ethanol, suspended in 20 µl sterile deionized water and then stored at −20°C.

Twenty-five samples of DNA ^{13}C-SIP experiment incubated with and without amendment of ^{12}C-*S. costatum* were sequenced. The V4 region of the bacterial and archaeal 16S rRNA genes were amplified using universal primer sets (Caporaso et al. 2012), 515F-Y (5′-GTG YCA GCM GCC GCG GTA A-3′;

Parada et al. 2016) and 806RB (5′-GGA CTA CNV GGG TWT CTA AT-3′; Apprill et al. 2015) (0.5 µM) and 2.5 U TaKaRa PrimeSTAR® GXL DNA polymerase (OZYME) in reactional system of 50 µl as described in Garel et al. (2019). The 16S amplicons were sequenced by the MiSeq Illumina (paired end 2 × 250 bp) platform Get of Genotoul (INRA, https://get.genotoul.fr).

2.6. Sequence data processing

The program 'dada2' (version 1.18) (Callahan et al. 2016) using default settings to correct sequence errors, in the R software version 3.4.3) was used to identify unique amplicon sequence variants (ASVs) from raw sequence reads. Using the function 'filterAndTrim', forward and reverse primer sequences were removed, maxEE was set to 2, trunQ was set to 11, maxN was set to 0. The function 'orient.fwd' was used to orient sequences in the same direction. Error rates of forward and reverse reads were modeled with 'learnerrors' for 100 million bases. Paired ends were merged with 'mergePairs' and unique sequences were inferred with the function 'dada'. Chimeras were removed with 'removeBimeraDenovo' using the 'consensus' method. Taxonomy was assigned to the output sequences through the Silva database (version 138; Quast et al. 2013). The 'phyloseq' package (McMurdie & Holmes 2013) was used to combine, analyze, and graphically display ASV tables. Raw sequence data were deposited to BioProject PRJ NA944440 (accession numbers SAMN33748629 to SAMN33748678)

To select the more differentially abundant genera, data were first converted in percentage with the 'transform_sample_counts' function from 'phyloseq' package version 1.16.2 and then aggregated by genus with 'aggregate_taxa' from the same package. To detect difference, another filter was used with 'Aggregate_rare' function followed by the parameters of detection equal to 1/100 and prevalence equal to 66/100. To visualize associations between different sources of data sets and reveal potential patterns 'ComplexHeatmap' package was applied. Vizualisation was based on the *z*-score of each genus (i.e. the distance from the mean abundance, expressed in number of standard deviations, by row). A boxplot representing the relative abundance of each genus (expressed as log) was generated and included on the heatmap plot, by the 'row_anno_boxplot' and 'rowAnnotation' functions.

Co-occurrence networks were built from the communities incubated in the presence of ^{12}C-*S. costatum*. The network analysis used in inputs data converted in percentage with 'transform_sample_counts' function. Only specific phyla were selected: *Proteobacteria*, *Bacteroidota*, *Planctomycetota*, *Cyanobacteria* and *Verrumicrobiota*. Three networks were computed, one for each density band (A, B and C, and D and E). The data were correlated using the 'trans_network' function from 'microeco' version 0.4.0 (Liu et al. 2021).

The calculation of the correlation was carried out with WGCNA (Langfelder & Horvath 2008) with a threshold equal to 0.0001 and Spearman for the method of the correlation. Only correlations with a coefficient (rho) > |0.7| were considered for further analysis. To visualize the network, Gephi software version 0.9 was used (Bastian et al. 2009). Nodes represented genera and edges represented the significant correlations between them. The network was defined by weighted correlation network analysis that determined modules (cluster of highly co-occurring microorganisms) and network nodes with regard to module membership.

Specific biodegradation response of the modules was assessed by Spearman's correlations between module eigengenes and the rate of biodegradation of selected compounds eicosanoic acid, docosanoic acid, 9,10-epoxy-18-hydroxyoctadecanoic acid (constituent of vegetable cuticular waxes), phytol, sitosterol, isomeric dihydroxyhexadecanoic acids (constituents of vegetable cuticular waxes), tetracosan-1-ol; hexacosan-1-ol, octacosan-1-ol, and triacontan-1-ol. To correlate the module and biodegradation rates, the package 'microeco' was used again with the functions 'cal_cor' to calculate and 'plot_cor' to visualize.

3. RESULTS

3.1. Lipid composition of *Avena sativa* leaves

The main ^{13}C labelled lipid components detected after alkaline hydrolysis of *A. sativa* leaves were hexadecanoic (palmitic), 3-(4-hydroxy-3-methoxyphenyl)prop-2-enoic (ferulic), and (2*E*)-3-(4-hydroxyphenyl)prop-2-enoic (*p*-coumaric) acids (Fig. 1). Smaller amounts of labelled long-chain fatty acids ($C_{20:0}$ and $C_{22:0}$), long-chain *n*-alkan-1-ols (C_{24}–C_{30}), phytol (chlorophyll phytyl side-chain), sitosterol, isomeric 9,16- and 10,16-dihydroxyhexadecanoic acids, degradation products of 9,10-epoxy-18-hydroxyoctadecanoic acid and traces of β-amyrin could be also

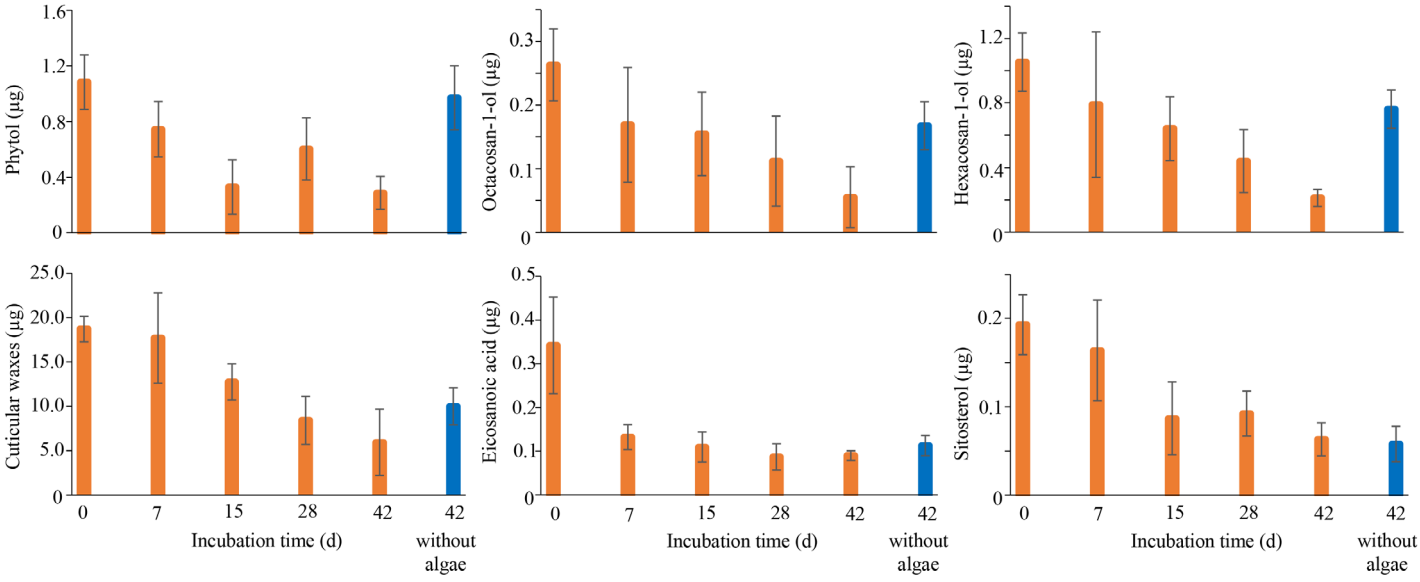

Fig. 1. Degradation of lipid components of ^{13}C-labelled *Avena sativa* during the incubations

detected (Table S1 in the Supplement at www.int-res.com/articles/suppl/a089p099_supp.pdf).

3.2. Degradation of ^{13}C-lipid components of *A. sativa*

^{13}C-labelled lipids were quantified after 0, 7, 15, 28 and 42 d of incubation (Fig. 1, Table S1). Degradation of fatty acids, *n*-alkan-1-ols, phytol, sitosterol, and components of cuticular waxes was observed. Interestingly, this degradation occurred without the accumulation of any detectable intermediate catabolites, likely due to their rapid remineralization (e.g. Boetius & Lochte 1996) or very low concentrations (i.e. less than the detection limit of the GC-QTOF). The degradation of phytol, C_{24}, C_{26} and C_{28} *n*-alkan-1-ols in controls (without diatoms) incubated for 42 d, appears to not be significant relative to initial time (T_0 = 0 d) (Table S2), whereas in treatments with diatoms these compounds were clearly degraded (3.5, 2.5, 5.5 and 2.5 times lower relative to T_0, respectively), (*t*-test, p = 0.01, p = 0.01, p = 0.002, p = 0.03, respectively, all < 0.05). Conversely, the decay of C_{20} and C_{22} fatty acids, cuticular waxes and sitosterol was significant in comparison with T_0 (Table S2) but unaffected by the presence of diatoms (*t*-test, p = 0.19, p = 0.21, p = 0.19, p = 0.75, respectively, all > 0.05) (Fig. 1, Table S2). There was also no detectable degradation of β-amyrin in any of the incubations.

3.3. Chemotaxonomy from ^{13}C bacterial lipids

To better characterize the bacteria involved in the assimilation of the labelled substrates, ^{13}C-incorporation (%) in specific bacterial fatty acids (Fig. 2) and hydroxyacids (Fig. 3) was measured during the experiment. This chemotaxonomic approach allowed us to determine which bacteria were involved in the degradation of the ^{13}C-labelled substrate (Table 1). The labelling appeared to increase strongly in the case of dodecanoic (×7 at T_{28d}), 12-methyltridecanoic (iso-C_{14}) (not present at T_0), 13-methyltetradecanoic (iso-C_{15}) (×34 at T_{28d}), hexadec-11-enoic (not present at T_0), 2-hydroxy-13-methyltetradecanoic (×18 at T_{28d}), 3-hydroxy-13-methyl-tetradecanoic (not present at T_0), octadec-11-enoic (×5 at T_{28d}) and 3-hydroxy-15-methylhexadecanoic (not present at T_0) acids.

3.4. Bacterial biodiversity in ^{13}C-*A. sativa* biodegradation experiments with or without ^{12}C-*Skeletonema costatum* as co-substrate

DNA-SIP was applied to track bacteria that assimilated ^{13}C-*A. sativa*. DNA fractions of increasing density were separated from each sample and submitted to Mi-seq sequencing. The density of all fractions ranged between 1.68 and 1.77 g ml^{-1}, with a linear trend increasing from the top to the bottom, indicating proper gradient formation. Five fractions of DNA

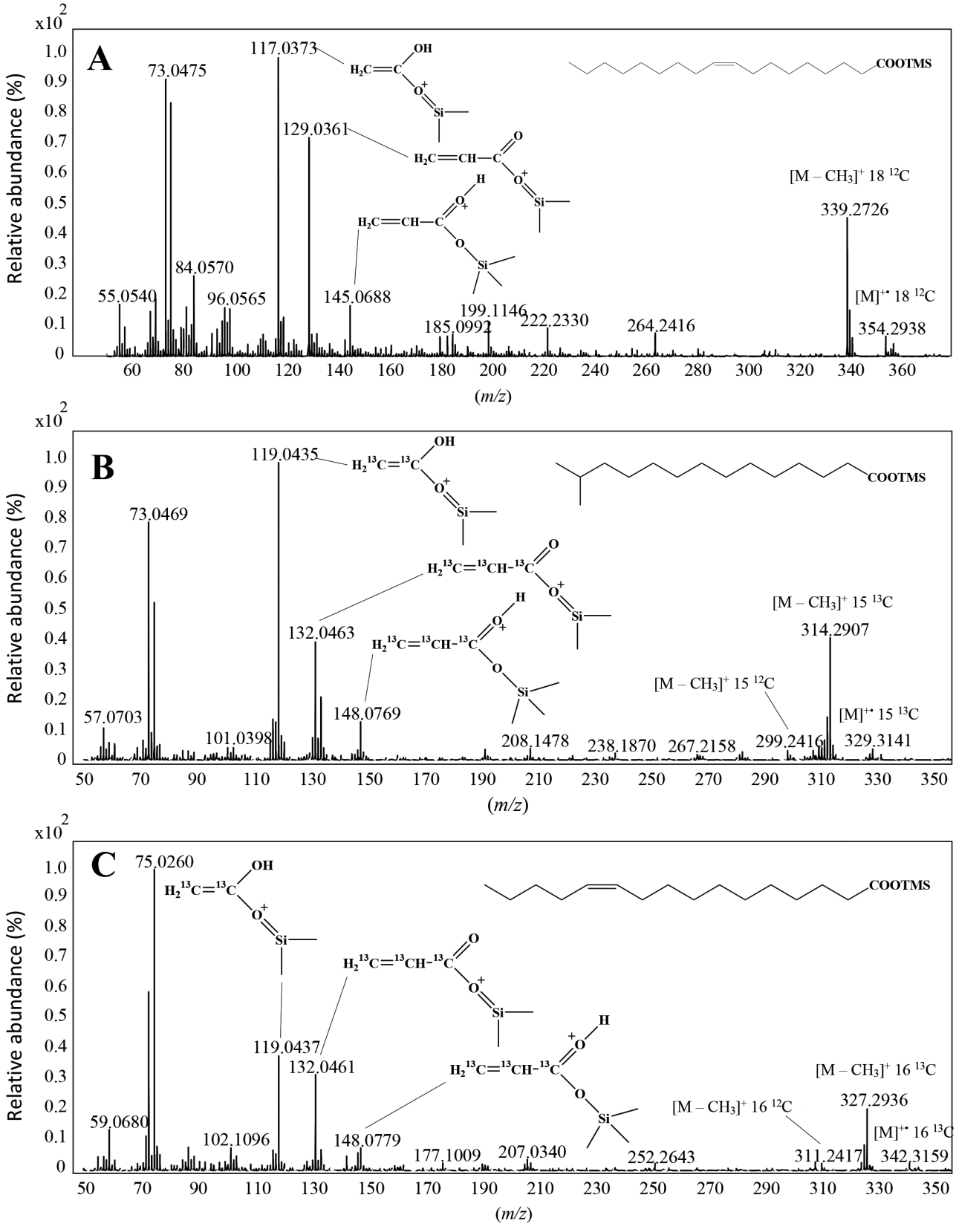

Fig. 2. Time-of-flight mass spectra (TOF MS) of (A) octadec-9-enoic, (B) 13-methyltetradecanoic, and (C) hexadec-11-enoic acid TMS derivatives at the end of the incubation. TMS: trimethylsilyl

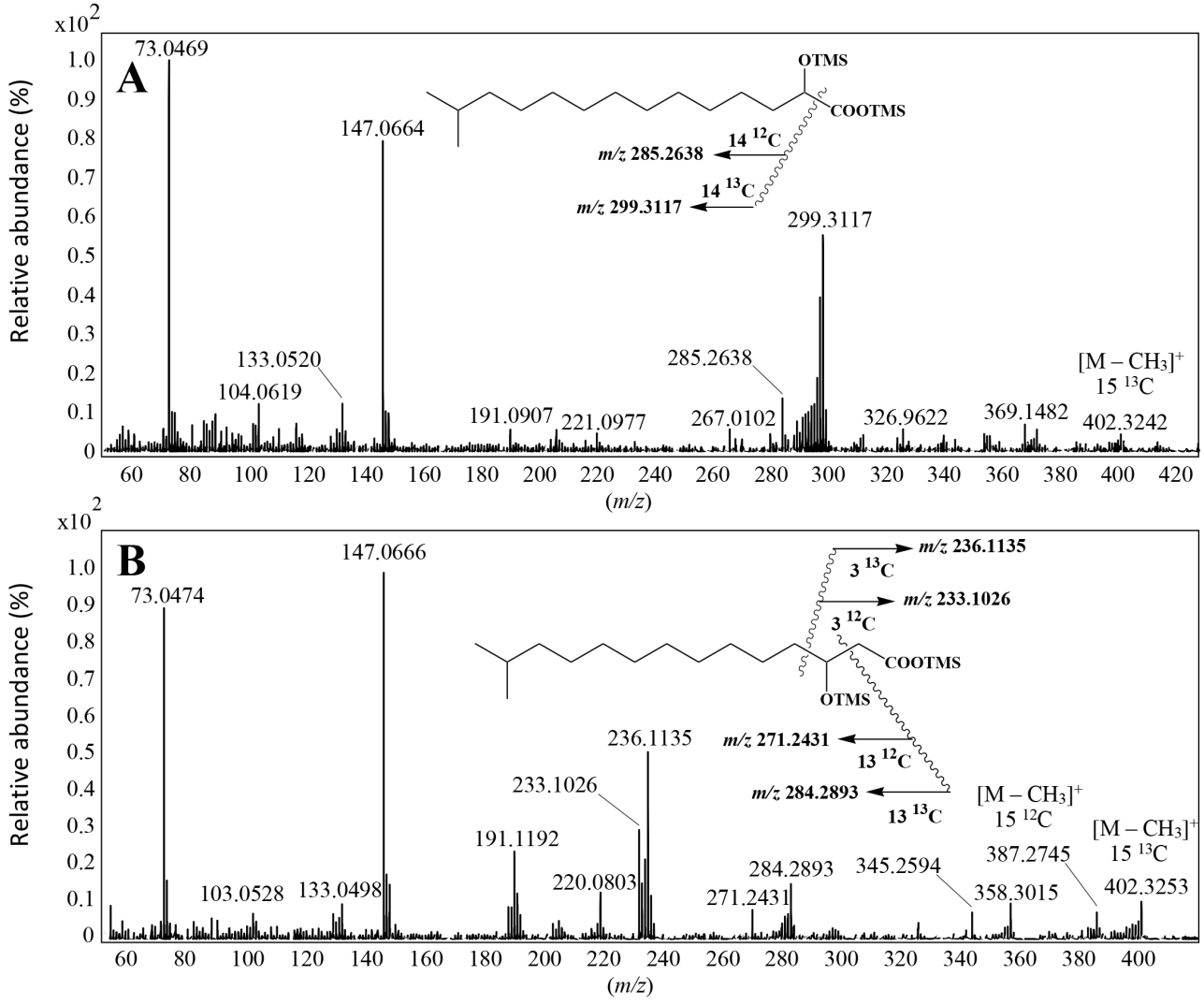

Fig. 3. Time-of-flight mass spectra (TOF MS) of (A) 2-hydroxy-13-methyltetradecanoic acid and (B) 3-hydroxy-13-methyltetradecanoic acid TMS derivatives at the end of the incubation

Table 1. ^{13}C incorporation (%) (after correction for natural ^{13}C abundance) in the main fatty acids during the incubation with algal cosubstrate (mean ± SD). nd: not detected

Fatty acids	Initial time	Incubation for 28 d	Incubation for 42 d
Dodecanoic acid	6.0 ± 1.0	42.3 ± 5.9	9.4 ± 3.8
Tetradecanoic acid	7.6 ± 0.6	9.4 ± 1.6	7.0 ± 0.8
Hexadecanoic acid	6.4 ± 1.1	3.9 ± 0.6	4.1 ± 0.7
Octadecanoic acid	9.5 ± 1.0	2.3 ± 0.1	2.7 ± 0.1
12-methyltridecanoic acid (iso C14)	nd	37.3 ± 4.3	39.0 ± 3.4
13-methyltetradecanoic acid (iso C15)	1.9 ± 0.6	64.8 ± 7.9	64.5 ± 1.1
12-methyltetradecanoic acid (anteiso C15)	0.9 ± 0.3	20.1 ± 3.4	22.3 ± 2.4
Hexadec-9-enoic acid	3.6 ± 0.2	35.0 ± 4.6	26.4 ± 1.5
Hexadec-11-enoic acid	nd	80.2 ± 3.6	78.5 ± 2.4
Octadec-9-enoic acid	14.1 ± 1.4	7.0 ± 1.5	11.0 ± 2.0
Octadec-11-enoic acid	6.6 ± 0.8	34.6 ± 8.0	29.2 ± 1.9
3-hydroxydecanoic acid	nd	24.1 ± 2.6	19.8 ± 6.7
3-hydroxytetradecanoic acid	10.0 ± 3.0	14.7 ± 2.4	7.3 ± 0.8
3-hydroxy-13-methyltetradecanoic acid	nd	69.6 ± 4.9	61.3 ± 2.0
3-hydroxyhexadecanoic acid	7.7 ± 1.5	19.4 ± 1.6	15.3 ± 1.1
3-hydroxy-15-methylhexadecanoic acid	nd	58.9 ± 6.6	56.3 ± 1.8
2-hydroxy-13-methyltetradecanoic acid	3.4 ± 1.1	72.4 ± 7.6	65.9 ± 2.0

were obtained from the heaviest (E, ^{13}C assimilating microorganisms) to the lightest (A, ^{12}C assimilating microorganisms) with BDs of ~1.755–1.740, 1.740–1.730, 1.730–1.720, 1.720–1.710 and 1.710–1.700 g ml^{-1}. Density fractions are indicated as H: heavy (D and E), M: medium (B and C), and L: light (A).

From 25 density fractions 1 207 563 raw reads were generated, ranging between 88 709 and 20 773 sequences per library (Table S3). After the quality trimming process, about 515 689 reads were retained (86%). The Good's index showed that the sequencing depths were sufficient to cover 97.8 ± 3.3% of the microbial diversity and the rarefaction curves approached saturation, indicating an acceptable sequencing depth for all remaining samples. All good quality sequences were distributed into 5164 ASVs. The global species richness (observed ASV counts) ranged from 54 to 106 ASVs depending on the sample.

Phylum-level phylogenetic analysis of communities incubated with the ^{12}C-diatom *S. costatum* as co-substrate (Fig. 4A, Table S4) indicated that sequences affiliated with *Bacteroidota* were highly abundant in the medium fractions (M, B and C: 1.710–1.730 g ml^{-1}) with a mean relative abundance of 47.01 ± 8.5%, which was 3.1–3.4 times higher than the lightest fraction (L, A) and the mean at T_0. In the heaviest fraction (H, D and E: 1.7230–1.755 g ml^{-1}), *Bacteroidota* abundance was close to that observed in the L fraction (21.2 ± 4.9 and 15.3 ± 3.8%, respectively). Although we observed a significant difference in the relative abundance of *Bacteroidota* among density fractions (ANOVA, *F*-value = 8743, p = 0.004), there was no significant effect of the presence of diatoms or incubation time (p = 0.561 and 0.181, respectively). In the same way, the relative abundance of *Proteobacteria* varied by density fraction (lower values in M fraction, ANOVA, *F*-value = 8743, p = 0.004) but only slightly over the incubation period (78.8 ± 6.1, 44.1 ± 9.3 and 57.8 ± 7.5% for the L, M and H fractions, respectively; ANOVA, *F*-value = 0, 243, p = 0.630). In the H fraction, the relative abundance of *Planctomycetota* and *Verrumicrobiota* reached 12.8 ± 2.7% (8-fold higher than in L fraction) and 6.5 ± 1.7%, respectively, after 28 d of incubation.

Among *Proteobacteria*, *Gammaproteobacteria* were dominant in the L fraction and thus used mainly the unlabeled algal substrate as a carbon source (Fig. 4A, Table S3), whereas *Alphaproteobacteria*, mainly found in the H fraction (Fig. 4B, Table S3), had clearly consumed the labelled *A. sativa*. *Gammaproteobacteria*, bacteria affiliated with *Nitrosococcales*, formerly affiliated with *Betaproteobacteria* (Fig. 4C), were most abundant in the L fraction and increased after 14 d to reach their maximal level (55.5 ± 4.6% of the total community). The same pattern was observed for the less abundant *Salinisphaerales*. For the other bacteria belonging to *Alteromonadales*, *Burkholderiales*, *Cellvibrionales*, and *Oceanospirillales* orders, no significant differences in their distribution in the incubation with diatoms or within fractions and over the incubation period was observed. In contrast, the relative abundance of *Alphaproteobacteria* (Fig. 4C) declined with time in the L fraction, but was maintained in H fractions. *Rhizobiales* and *Sphingomonadales* orders were significantly higher in abundance in the H fraction with 47.2 (H-42 d)-fold higher abundance than those of the L fraction for the former and 61.6 (H-28 d)-fold for the latter. A significant effect of diatom addition was only observed with *Rhizobiales* (*t*-test, n = 10, p = 0.023).

Among *Bacteroidota*, the relative abundance of *Flavobacteriales* (Fig. 4D) reached its highest value in the M fraction from 14 d of incubation (32.4 ± 5.3%), whereas *Cytophagales* overabundances were observed from only 7 d (18.9 ± 5.6%). In the M fraction (B band), after 14 d of incubation, *Flavobacteriales* and *Cytophagales* were more abundant in the incubation with diatom addition with increasing relative abundance of up to 3.6 and 14.3 times, respectively. In the H fraction, their abundances (10.6 ± 3.3% and 3.1 ± 2.7%, respectively) were clearly weaker (Fig. 3D), and the significance was low, most likely due to the small number of samples (*t*-test, n = 4, p = 0.051, p = 0.106 for *Cytophagales* and *Flavobacteriales*, respectively).

3.5. Differentially abundant genera in the presence of diatoms

To disentangle the effect of *S. costatum* as an algal co-substrate on various genera of the community, we focused on the 2 main phyla (*Proteobacteria* and *Bacteroidota*). We identified which genera had significantly different relative abundances between incubations with and without the diatom, *S. costatum* for the same sampling times (14 and 42 d) and for the L, M and H fractions, respectively (Fig. 5). The *z*-score pattern of the most discriminant genera has been used to highlight the clear effect of *S. costatum* as a co-substrate that influences bacterial diversity.

Looking across the whole community, the presence of diatoms only affected the relative abundance of a few genera. Except *Methylophaga*, whose relative abundance reached up to 45% of

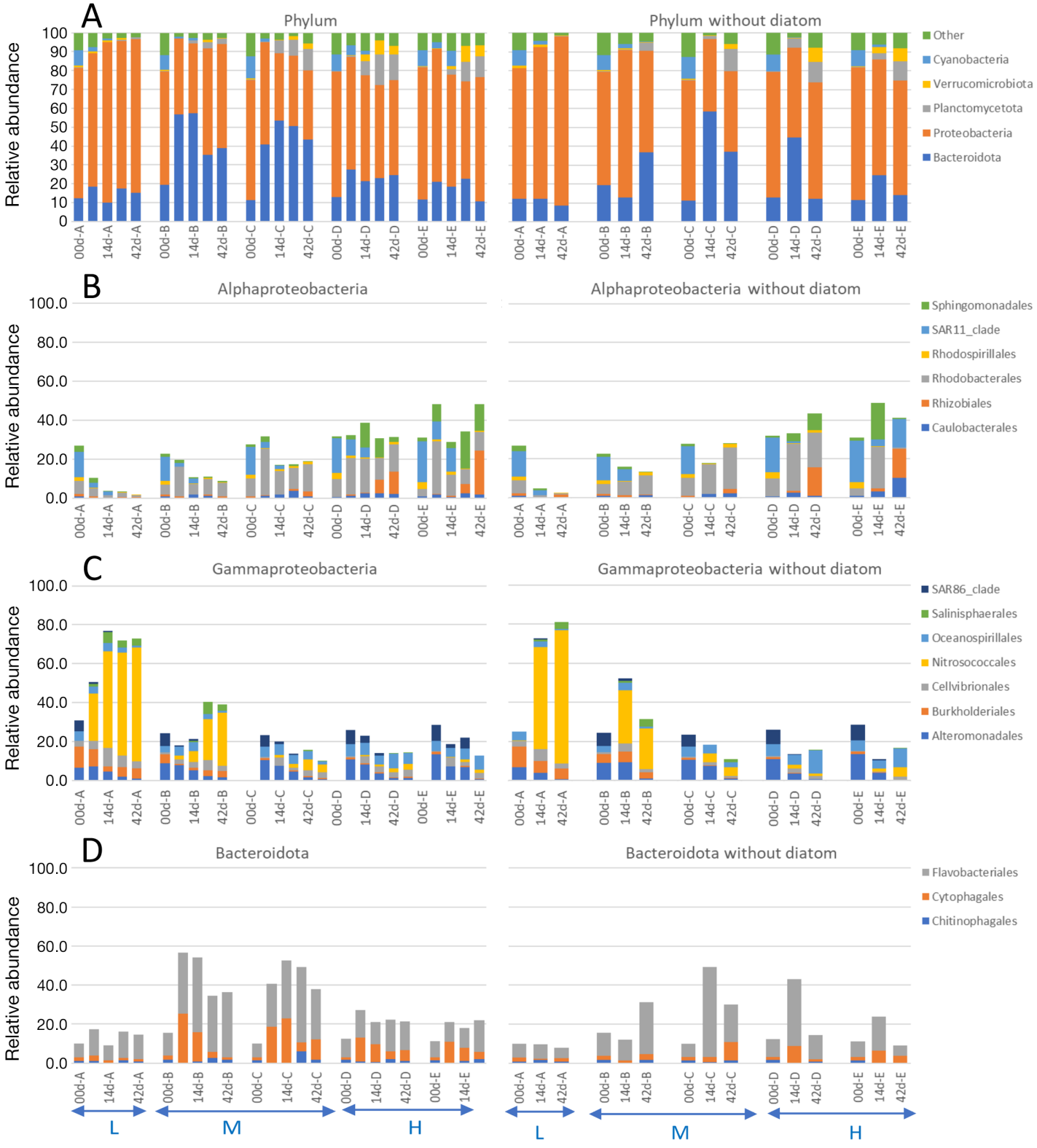

Fig. 4. Taxonomic affiliation (A) amongst the 5 most abundant phyla, (B) within the class *Alphaproteobacteria*, (C) withinthe class *Gammaproteobacteria*, and (D) within the phylum *Bacteroidota* obtained from the 16*S* rRNA gene (DNA) sequences at different sampling times during the incubation with (left) or without (right) diatom amendment. The group 'Other' contains all phyla with relative abundance lower than 1% of the total community. A–E correspond to the lightest and heaviest density fractions of DNA. Density fractions are indicated as H: heavy (D and E), M: medium (B and C), and L: light (A)

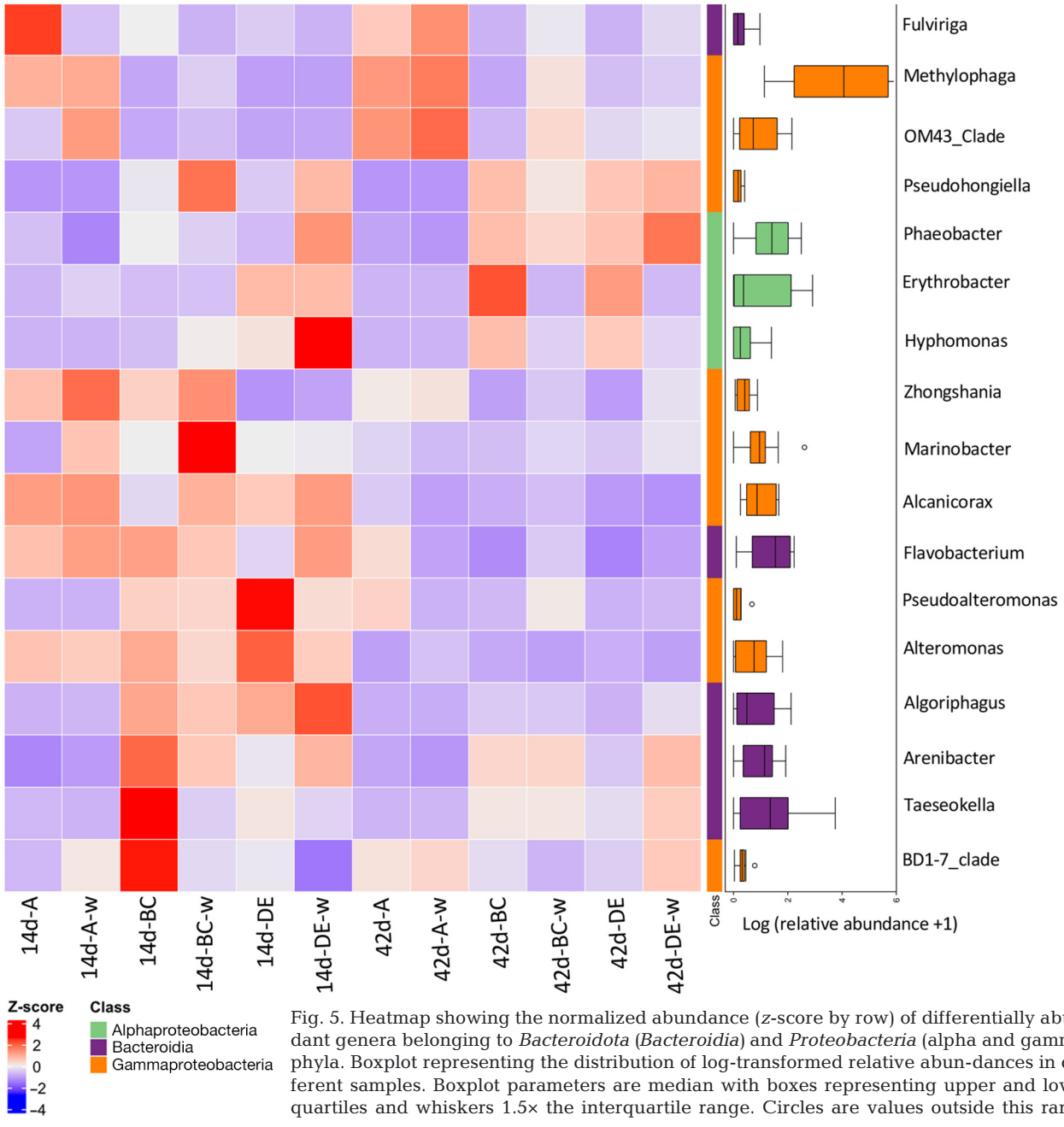

Fig. 5. Heatmap showing the normalized abundance (*z*-score by row) of differentially abundant genera belonging to *Bacteroidota* (*Bacteroidia*) and *Proteobacteria* (alpha and gamma) phyla. Boxplot representing the distribution of log-transformed relative abun-dances in different samples. Boxplot parameters are median with boxes representing upper and lower quartiles and whiskers 1.5× the interquartile range. Circles are values outside this range

the total community in band A, the genera differentially abundant between incubations with and without diatoms were minor and their relative abundance rarely exceeded 1%. After 14 d of incubation, in the M bands the *Taeseokella, Algoriphagus* and *Flavobacterium* genera belonging to the *Bacteroidota* were significantly more abundant in the presence of diatoms, while in the H bands *Alteromonas* and *Pseudoalteromonas* were dominant (Fig. 5). After 42 d, only *Erythrobacter* was more abundant in the diatom incubations.

3.6. Co-occurence network analysis

Recent studies showed that microbial co-occurrence patterns can help reveal ecologically meaningful interactions between species (Steele et al. 2011). To further investigate the potential microbial consortia implicated in the priming of TPOM in the presence of diatoms, co-occurrence networks were constructed. We built a co-occurrence network that was based on strong and significant Spearman rank correlations. Network analyses have shown that co-

occurring species are frequently arranged in groups, or modules, with a particular functional relevance (Chaffron et al. 2010, Barberan et al. 2012). Correlations between modules and the rates of biodegradation of ^{13}C-specific compounds were calculated (Fig. 6).

As expected, in the lightest band (L) there was no correlation between any module and the degradation of ^{13}C-TPOM markers (Fig. 6A). The intermediate fractions M, contained DNA of bacteria that assimilated both ^{13}C-labelled *A. sativa* and ^{12}C-*S. costatum* and thus played a potential role in the observed priming effects (Fig. 6B). Modules M6, M21 and M13 representing 5.15, 2.84 and 0.42% of the network nodes (Fig. S1A), were significantly correlated with the degradation of most of the TPOM markers (Fig. 6C). A strong correlation was observed between these 3 modules and the increase in degradation rates of octacosan-1-ol and phytol (except M21) in the presence of diatoms. The microorganisms associated with these 3 modules also appeared to be associated with the degradation of triacontan-1-ol, eicosanoic acid and docosanoic acid without being stimulated by the addition of diatoms. M13 was significantly correlated with the degradation of most TPOM markers including octacosan-1-ol (*), tetracosan-1-ol (*), hexacosan-1-ol (**), dihydroxy-16,(9/10)-hexadecanoic acids (*) and phytol (*), whose degradation was stimulated in the presence of diatoms providing some evidence for a priming effect.

Module M6 grouped 21 ASV affiliated to SAR order and 3ASVs belonging to *Flavobacteriales* (*Flavobacterium* and NS-marine group). Amongst *Alphaproteobacteria*, 5 ASVs are mainly affiliated to *Rhizobiales* and *Rhodobacterales* and for *Gammaproteobacteria* ASVs are affiliated to *Alteromonadales* and *Pseudomonadales*.

Within M13, 3 ASVs were distributed among *Bacteroidota* including genera belonging to *Flavobacteriales* order (NS-marine group, *Mesoflavibacter*) and *Cytophagales* order (*Marinoscillum*). 22 ASVs were associated with *Proteobacteria*, including 11 ASVs among *Alphaproteobacteria*: *Rhizobiales*, *Rhodobacterales* and *Sphingomonadales* (*Erythrobacter* and *Sphingorhabdus*) and 11 ASVs of *Gammaproteobacteria*, mainly *Alteromonadales* (*Alteromonas* genus; 6/11).

The heaviest fractions (H) concentrated the DNA of bacteria growing only on the ^{13}C-labelled *A. sativa* vascular plant and not on ^{12}C- *S. costatum*. Modules M9 and M23 representing 5.38 and 0.55% of the nodes of the network, respectively (Fig. 6D, Fig. S1B), showed significant correlations with biodegradation of TPOM differentially degraded in the presence of diatoms excepted for phytol and sitosterol (Fig. 6E). Module M9 also included 2 ASVs affiliated to *Bacteroidota* (*Flavobacteriales*, NS marine group); *Gammaproteobacteria* (11 ASV identified as *Alteromonas* and *Oceanospirillales*) and *Alphaproteobacteria* (22 ASVs including SAR11, *Rhodobacteraceae* and *Sphingomonadaceae*).

Module M23 grouped new genera belonging to *Bacteroidota* (*Aurantivirga, Mariniflexile* amongst *Flavobacteriales* order) and *Altererythrobacter* belonging to *Sphingomonadales*. Unexpectedly, none of the genera belonging *Rhizobiales* orders that were more abundant at the end of incubation in the H band were directly included in modules that correlate strongly with the rate of degradation of TPOM tracer compounds.

4. DISCUSSION

4.1. Lipid biomarkers of ^{13}C-*Avena sativa* leaves biodegradation

Quantification of labelled lipids allowed for the detection of *A. sativa* bacterial remineralization during the incubations, with *A. sativa* used as a model TPOM substrate. We excluded palmitic acid from our analyses, which may be produced by bacteria growing on ^{13}C-labelled substrates, and ferulic and *p*-coumaric acids, whose volatile TMS derivatives can be lost by evaporation during the silylation process. Moreover, the production of these 2 phenolic acids during biodegradation of biopolymers (Otto et al. 2005, Fazary & Ju 2007, Xu et al. 2018) clearly compromises interpretation of changes in the abundance of these compounds. We utilized the following labelled lipids to detect *A. sativa* remineralization: phytol, C_{24}–C_{28} alkan-1-ols, $C_{20:0}$ and $C_{22:0}$ fatty acids, sitosterol, β-amyrin and products of alkaline depolymerisation of cuticular waxes i.e. isomeric dihydroxyhexadecanoic acids (mainly 9,16- and 10,16-) and 9,10-epoxy-18-hydroxyoctadecanoic acid (Holloway & Deas 1973, Deas & Holloway 1977, Kolattukudy 1980), the epoxy group of the latter being converted to the corresponding methoxyhydrins, triols, and chlorohydrins during the treatment (Marchand & Rontani 2001) (Fig. S2). Incubations were carried out under aerobic conditions; hence, the effects of autoxidative processes on TPOM degradation could not be totally excluded. Autoxidation can operate in all oxic aquatic environments (Schaich 2005) and potentially affect all

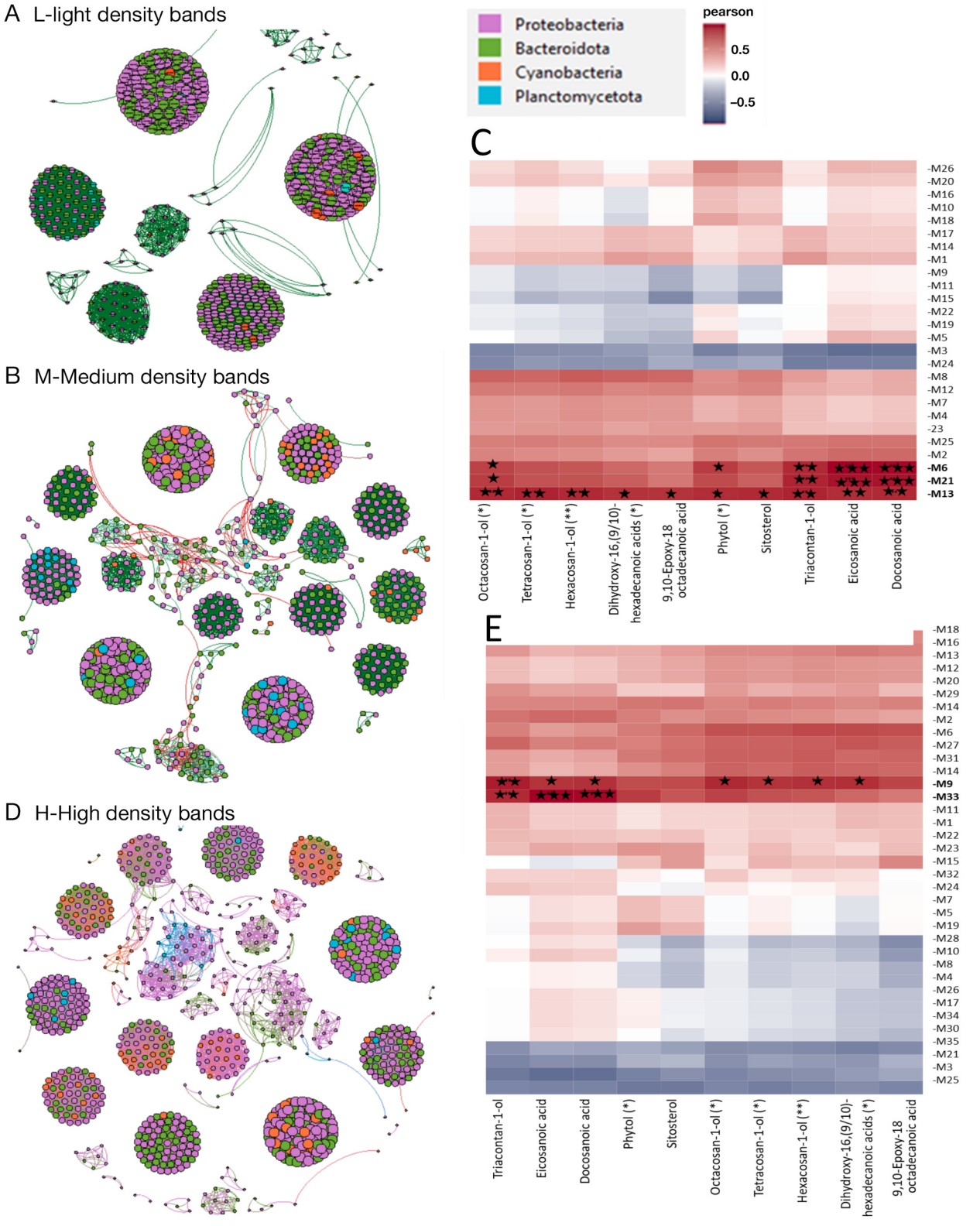

Fig. 6. Co-occurrence network based on correlation analysis. Each node denotes a microbial genera; node color denotes taxonomic classification. Edge lines between nodes represent significant co-occurrences relationships. Edge size indicates the strength of Spearman correlation among nodes. (A,B,D) Co-occurrence network of light, medium and heavy density bands, respectively; (C) and (E) show the correlations (Pearson, rho) between module eigengenes and environmental traits in the core community network. Red: highly positive correlation; blue: highly negative correlation. Stars next to the compound indicate compounds that are significantly differentially degraded in the presence of diatoms. Significance of p-values are indicated in plots and near the compounds: $p > 0.05$; $^{*}p \leq 0.05$; $^{**}p \leq 0.01$; $^{***}p \leq 0.001$

unsaturated lipids (Rontani 2012, Rontani & Belt 2020). However, the decrease in concentrations of 24-ethylcholesta-3β,5α,6β–triol and 3,7,11,15-tetramethyl-hexadec-2(*Z*/*E*)-en-1,4-diols (specific autoxidation products of sitosterol and phytol, respectively; Rontani & Aubert 2005, Rontani et al. 2014), provided evidence that observed lipid decay in the incubations was microbially mediated with no autoxidative artifact.

Examination of ^{13}C incorporation in octadec-9-enoic (oleic) acid (main fatty acid of fungi; Athenaki et al. 2018) and 13-methyltetradecanoic, hexadec-11-enoic, 2-hydroxy-13-methyltetradecanoic and 3-hydroxy-13-methyltetradecanoic acids (fatty and hydroxy acids specific to bacteria; Fautz et al. 1979, Harwood & Russell 1984, Blumenberg et al. 2005) (Figs. 2 & 3) clearly demonstrated that the primary microbes responsible for the assimilation of ^{13}C-labelled *A. sativa* were bacteria. The lack of labelled archaeol (well-known tracer of *Archaea*; Šuštar et al. 2012) during the incubation and SIP results (see Fig. 2 where *Archaea* are in the 'other' phylum) do not support the involvement of *Archaea* in the degradation of *A. sativa*.

4.2. Direct evidence of priming effects

The lack of bacterial degradation of some ^{13}C-labelled *A. sativa* lipids (phytol, C_{24}–C_{30} alkanols and cuticular waxes) in the absence of ^{12}C-*S. costatum* and their significant increases after addition of the diatom (Fig. 1, Table S1, Fig. S2), provides evidence of positive priming effects (Bianchi et al. 2011, Guenet et al. 2018). However, it is interesting to note that this enhanced degradation in the presence of diatoms was not observed for C_{20} and C_{22} fatty acids and sitosterol (Fig. 1, Table S1). Interestingly, this shows that efficiency of a possible priming effect is targeted to certain compounds in vascular plants, something that will clearly help in resolving some inconsistencies in past priming studies (see Bengtsson et al. 2018, Sanches et al. 2021).

In particular, the compounds-specific selectivity of priming effects may be attributed to (1) an increase of the biomass of specific bacteria resulting from the consumption of reactive substrates, such as algal fatty acids, amino acids and sugars (Grant & Betts 2004), or (2) an enhanced microbial production of extracellular enzymes able to degrade some *A. sativa* components, driven by the degradation of algal priming components (Ward et al. 2016, Guenet et al. 2018). We posit these results are in good agreement with (1) the strong degradation of TPOM previously observed during incubations of Rhône SPM containing a high proportion of freshwater diatoms in seawater (Bonin et al. 2019), and (2) the increase of bacterial degradation of vascular plant material with the proportion of algal sterols, observed in SPM samples collected in the salinity gradient of the Rhône Estuary (Bonin et al. 2019). Observations of enhanced microbial respiration at the confluence of turbid and clear waters of the Amazon River revealed similar findings (Ward et al. 2019a). Thus, the incubation experiment indirectly supports previous speculations by Bonin et al. (2019) that priming may have been occurring across similar steep turbidity and algal gradients in the Rhône Estuary. High rates of lipid decomposition are similarly observed in other dynamic settings where diverse processes occur, such as newly deposited material at the estuarine and marine sediment interfaces (Canuel & Martens 1996, Sun et al. 2000), remineralization of sinking particles (Meyers & Eadie 1993), and turbidity currents (Treignier et al. 2006). These are all environmental settings where priming effects could potentially occur (e.g. Aller & Cochran 2019), though have not necessarily been frequently observed based on experimental techniques applied to date (Bengtsson et al. 2018).

4.3. Bacterial consortium responsible for *A. sativa* driving biodegradation

The use of stable isotope tracers enables us to link the identity of microorganisms to their biogeochemical function in both field and lab studies. In this study, we explored for the first time the stimulation of the mineralization of *A. sativa,* as a model TPOM substrate labelled with ^{13}C, via priming with marine diatoms to better elucidate the dynamics and identity of microbial populations that actively assimilated the carbon of residue during its degradation process.

In the case of our observations of different relative abundances of some genera under different incubation conditions, we note that the microbial communities are very different across the different density fractions (L, M and H) showing a specificity of the used organic matter. The most striking differences were observed in the lightest fraction where *Gammaproteobacteria* were dominant. These opportunistic copiotroph organisms took advantage of the fresh organic matter supply. In contrast, we did not observe clear modification of the biodiversity of

microorganisms that assimilated ^{13}C-*A. sativa* at the phylum level in M and H fractions, whereas the biodegradation of ^{13}C-lipids was very strongly stimulated.

In the intermediary band (M), *Flavobacteriales* and *Cytophagales* were most abundant in the bacterial community that assimilated both ^{13}C-labelled *A. sativa* and ^{12}C- *S. costatum* and could have played a role in priming. After 14 d of incubation, the addition of ^{12}C-*S. costatum* led to a dominance of *Bacteroidota* (*Flavobacterium, Arenibacter* and *Taeseokella*), followed by *Alphaproteobacteria* (*Erythrobacter* and *Hyphomonas*) after 42 d. These different genera appear to have assimilated both carbon sources in the presence of diatoms but were not included in the main modules that had the highest correlation with the rate of ^{13}C-lipid biodegradation. The assimilation of ^{13}C-*A. sativa* by *Bacteroidota* was further supported by chemotaxonomy. For instance, bacteria of the *Cytophagales* order were characterized by a high content of iso-C_{15}, hexadec-11-enoic, 3-hydroxy-13-methyltetradecanoic and 3-hydroxy-15-methylhexadecanoic acids (McGrath et al. 1990, Nedashkovskaya et al. 2005), with the *Flavobacteria* genus dominated by iso-C_{15}, 2-hydroxy-13-methyltetradecanoic, 3-hydroxy-13-methyltetradecanoic and 3-hydroxy-15-methylhexadecanoic acids (Moss & Dees 1978, Zamora et al. 2013).

The high presence of these ^{13}C-labelled acids (Table 1) confirms that bacteria belonging to the *Bacteroidota* phylum strongly contributed to the remineralization of *A. sativa*. Members of the *Bacteroidota* phylum, specifically *Flavobacteria* and *Cytophaga*, are particularly common in estuaries (Crump et al. 1999, Böckelmann et al. 2000) and in the oceans (Kirchman 2002) and are also well known for their ability to catabolize polyaromatic substances (e.g. lignin) and sugar polymers (e.g. hemicellulose) from higher plants (Kisand et al. 2002) due to the presence of specific profiles of hydrolytic enzymes. They can also utilize lipids, proteins, and DNA present in dead organisms (O'Sullivan et al. 2002). Moreover, members of the *Bacteroidota* phylum exhibit gliding motility and are therefore thought to live primarily on surfaces (DeLong et al. 1993, Riemann et al. 2000). Thus, they seem to be the ideal organisms to thrive as particle-attached bacteria in the estuaries (Crump et al. 1999), an attribute that has been suggested to play an important role in priming (Catalán et al. 2015). Moreover, Teeling et al. (2012) previously observed that such bacteria responded first to the available substrates from dying diatoms and increased rapidly in cell numbers. As such, bacteria belonging to this phylum should thus play a key role in the production of the biomass needed for carrying out priming effects.

The part of the microbial community that primarily consumed the ^{13}C-*A. sativa* TPOM tracer was found in the densest band (H). The modules showing a strong correlation with the lipid tracers are composed of the same genera as the modules identified in the intermediate density band, *Flavobacteriales* (NS marine group), and *Gammaproteobacteria* (*Alteromonas*, *Pseudoalteromonas* and *Marinobacter*). Bacteria belonging to these genera seem to play a major role in the degradation and assimilation of the lipid fraction of TPOM. In this fraction, a significant increase in the abundance of *Sphingomonadales* and *Rhizobiales* was also observed and likely contributed to the degradation of ^{13}C-*A. sativa* (Fig. 4). The lack of correlation between the degradation of ^{13}C-labelled lipid tracers and the abundance of these bacteria suggests that these organisms mainly grew on non-lipidic ^{13}C-labelled components of *A. sativa* (e.g. sugars, proteins, lignocellulose and lignin). It is interesting to note that *Sphingomonas paucimobilis* SYK-6, which is one of the most well-characterized lignin-degrading bacteria (Masai et al. 1999), produces specific enzymes, such as β-etherases, O-demethylases, and ring fission dioxygenases, which are essential in the lignin decomposition metabolic pathway (Jeffries 1991, Sonoki et al. 2002, Bugg et al. 2011).

The presence of such enzymes in *Sphingomonadales* makes these species particularly well adapted to the degradation of higher plant material. *Rhizobium* species, which are widely distributed in nature and are usually isolated from the plant rhizosphere (Yoon et al. 2010, Sun et al. 2013), also possess the genomic and physiological capability to metabolize lignin and lignin-like compounds (Jackson et al. 2017). Due to the simultaneous presence of lignin-oxidizing and carbohydrate-hydrolyzing genes in *Rhizobiales* (Jackson et al. 2017), these bacteria are also able to efficiently degrade lignocellulose. However, ^{13}C-incorporation in fatty acids of *Sphingomonadales* and *Rhizobiales* could not be measured by the analytical techniques used here. *Sphingomonadales* are generally characterized by the presence of sphingolipids and 2-hydroxyacids (Busse et al. 1999). The 2-hydroxyacids, linked to sphingosine by amide bonds, are only very weakly hydrolyzed during the alkaline hydrolysis step employed during the treatment. The preponderance of amide-linked fatty acids is also a characteristic of *Rhizobiales* (Russa et al. 1995).

5. CONCLUSIONS

Incubation of ^{13}C-labelled *Avena sativa* leaf debris as a model TPOM substrate in seawater with Rhône SPM as inoculum showed an enhancement of the decomposition of some *A. sativa* lipid components (phytol, *n*-alkan-1-ols and cuticular waxes) in the presence of diatoms (*Skeletonema costatum*). Diatom amendment did not affect the degradation of other lipids (fatty acids and sitosterol), suggesting that positive priming effects may have compound-specific selectivity. Using molecular markers, we were able to identify that bacteria of the *Bacteroidota* phylum played a dominant role in priming-induced TPOM degradation in estuarine waters. Priming of TPOM was carried out by a consortium of microbes (mainly *Flavobacteria* and *Cytophaga*) after consumption of labile substrates. *Sphingomonadales* and *Rhizobiales* microbes that possess enzymes needed for lignin and hemicellulose metabolism may also contribute to TPOM degradation in aquatic environments. However, in the case of this experiment their abundance was not stimulated by the presence of algal substrates. These results suggest an apparent priming effect that resulted from synergistic interactions between different bacterial groups, each utilizing different substrates, in contrast to priming associated with a single bacterial population utilizing both algal and higher plant materials (Bianchi et al. 2015).

Future research should further evaluate the underlying mechanisms by which priming effects vary along salinity and river-mouth or continental-shelf gradients to further constrain the fate of terrigenous material in the coastal zone. Likewise, it is critical to explore the impact of increasing coastal eutrophication on the decomposition of TPOM, both as it is delivered from rivers to the sea and after being stored in coastal sediments.

Acknowledgements. This study was carried out in the framework of the project BALTOMS, this work received support from the French government under the France 2030 investment plan, as part of the Initiative d'Excellence d'Aix-Marseille Université - A*MIDEX (AMX-19-IET-012). Thanks are due to the FEDER OCEANOMED (N° 1166-39417) for the funding of the apparatus employed and 2 anonymous reviewers for their useful and constructive comments.

LITERATURE CITED

Aller RC, Cochran JK (2019) The critical role of bioturbation for particle dynamics, priming potential, and organic C remineralization in marine sediments: local and basin scales. Front Earth Sci 7:157

Apprill A, McNally S, Parsons R, Weber L (2015) Minor revision to V4 region SSU rRNA 806R gene primer greatly increases detection of SAR11 bacterioplankton. Aquat Microb Ecol 75: 129–137

Athenaki M, Gardeli C, Diamantopoulou P, Tchakouteu SS, Sarris D, Philippoussis A, Papanikolaou S (2018) Lipids from yeasts and fungi: physiology, production and analytical considerations. J Appl Microbiol 124:336–367

Barberán A, Bates ST, Casamayor EO, Fierer N (2012) Using network analysis to explore co-occurrence patterns in soil microbial communities. ISME J 6:343–351

Bastian M, Heymann S, Jacomy M (2009) Gephi: an open source software for exploring and manipulating networks. Proc Int AAAI Conf Web Social Media 3:361–362

Bastida F, García C, Fierer N, Eldridge DJ and others (2019) Global ecological predictors of the soil priming effect. Nat Commun 10:3481

Bengtsson MM, Attermeyer K, Catalán N (2018) Interactive effects on organic matter processing from soils to the ocean: Are priming effects relevant in aquatic ecosystem? Hydrobiologia 822:1–17

Benner R, Maccubbin AE, Hodson RE (1984) Anaerobic biodegradation of the lignin and polysaccharide components of lignocellulose and synthetic lignin by sediment microflora. Appl Environ Microbiol 47:998–1004

Berner RA (1982) Burial of organic carbon and pyrite sulfur in the modern ocean: its geochemical and environmental significance. Am J Sci 282:451–473

Bianchi TS (2011) The role of terrestrially derived organic carbon in the coastal ocean: a changing paradigm and the priming effect. Proc Natl Soc Acad Sci USA 108: 19473–19481

Bianchi TS, Morrison E (2018) Human activities create corridors of change in aquatic zones. EOS 99:13–15

Bianchi TS, Wysocki LA, Schreiner KM, Filley TR, Corbett DR, Kolker AS (2011) Sources of terrestrial organic carbon in the Mississippi plume region: evidence for the importance of coastal marsh inputs. Aquat Geochem 17: 431–456

Bianchi TS, Goni M, Allison M, Chen N, McKee B (2013) Sedimentary carbon dynamics of the Atchafalaya and Mississippi River Delta system and associated margin. In: Bianchi TS, Allison MA, Cai WJ (eds) Biogeochemical dynamics at major river-coastal interfaces: linkages with global change. Cambridge University Press, Cambridge, p 473–502

Bianchi TS, Thornton DCO, Yvon-Lewis SA, King GM and others (2015) Positive priming of terrestrially derived dissolved organic matter in a freshwater microcosm system. Geophys Res Lett 42:5460–5467

Bianchi TS, Morrison E, Barry S, Arellano AR and others (2018) The fate and transport of allochthonous blue carbon in divergent coastal systems. In: Windham-Myers L, Crooks S, Troxler TG (eds) A blue carbon primer. CRC Press, Boca Raton, FL, p 25–48

Bianchi TS, Anand M, Bauch CT, Canfield DE and others (2021) Biogeochemistry: its future role in sustainability science. Biogeosciences 18:3005–3013

Björdal CG (2012) Microbial degradation of waterlogged archaeological wood. J Cult Herit 13:S118–S122

Björdal CG, Dayton PK (2020) First evidence of microbial wood degradation in the coastal waters of the Antarctic. Sci Rep 10:12774

Blanchette RA (2010) Microbial degradation of wood from aquatic and terrestrial environments. In: Mitchell R,

McNamara CJ (eds) Cultural heritage microbiology: fundamental studies in conservation science. ASM Press, Washington, DC, p 179–190

Blumenberg M, Seifert R, Nauhaus K, Pape T, Michaelis W (2005) In vitro study of lipid biosynthesis in an anaerobically methane-oxidizing microbial mat. Appl Environ Microbiol 71:4345–4351

Böckelmann U, Manz W, Neu TR, Szewzyk U (2000) Characterization of the microbial community of lotic organic aggregates ('river snow') in the Elbe River of Germany by cultivation and molecular methods. FEMS Microbiol Ecol 33:157–170

Boetius A, Lochte K (1996) Effect of organic enrichments on hydrolytic potentials and growth of bacteria in deep-sea sediments. Mar Ecol Prog Ser 140:239–250

Bonin P, Prime AH, Galeron MA, Guasco S, Rontani JF (2019) Enhanced biotic degradation of terrestrial POM in an estuarine salinity gradient: interactive effects of organic matter pools and changes of bacterial communities. Aquat Microb Ecol 83:147–159

Bourgeois S, Pruski AM, Sun MY, Buscail R and others (2011) Distribution and lability of land-derived organic matter in the surface sediments of the Rhône prodelta and the adjacent shelf (Mediterranean Sea, France): a multi proxy study. Biogeosciences 8:3107–3125

Bugg TDH, Ahmad M, Hardiman EM, Rahmanpour R (2011) Pathways for degradation of lignin in bacteria and fungi. Nat Prod Rep 28:1883–1896

Burdige DJ (2005) Burial of terrestrial organic matter in marine sediments: a re-assessment. Global Biogeochem Cycles 9:GB4011

Busse HJ, Kämpfer P, Denner EBM (1999) Chemotaxonomic characterisation of *Sphingomonas.* J Ind Microbiol Biotechnol 23:242–251

Callahan BJ, McMurdie PJ, Rosen MJ, Han AW, Johnson AJA, Holmes SP (2016) DADA2: high-resolution sample inference from Illumina amplicon data. Nat Methods 13: 581–583

Canuel EA, Martens CS (1996) Reactivity of recently deposited organic matter: degradation of lipid compounds near the sediment-water interface. Geochim Cosmochim Acta 60:1793–1806

Caporaso JG, Lauber CL, Walters WA, Berg-Lyons D and others (2012) Ultra-high-throughput microbial community analysis on the Illumina HiSeq and MiSeq platforms. ISME J 6:1621–1624

Catalán N, Kellerman AM, Peter H, Carmona F, Tranvik LJ (2015) Absence of a priming effect on dissolved organic carbon degradation in lake water. Limnol Oceanogr 60: 159–168

Chaffron S, Rehrauer H, Pernthaler J, Von Mering C (2010) A global network of coexisting microbes from environmental and whole-genome sequence data. Genome Res 20:947–959

Crump BC, Armbrust EV, Baross JA (1999) Phylogenetic analysis of particle-attached and free-living bacterial communities in the Columbia River, its estuary, and the adjacent coastal ocean. Appl Environ Microbiol 65: 3192–3204

de Leeuw JW, Largeau C (1993) A review of macromolecular organic compounds that comprise living organisms and their role in kerogen, coal, and petroleum formation. Org Geochem 11:23–72

Deas AHB, Holloway PJ (1977) The intermolecular structure of some plant cutins. In: Tevini M, Lichtenthaler HK (eds) Lipids and lipid polymers in higher plants. Springer, Berlin, p 293–299

DeLong EF, Franks DG, Alldredge AL (1993) Phylogenetic diversity of aggregate-attached vs. free-living marine bacterial assemblages. Limnol Oceanogr 38:924–934

Fautz E, Rosenfelder G, Grotjahn L (1979) Iso-branched 2- and 3-hydroxy fatty acids as characteristic lipid constituents of some gliding bacteria. J Bacteriol 140: 852–858

Fazary AE, Ju YH (2007) Feruloyl esterases as biotechnological tools: current and future perspectives. Acta Biochim Biophys Sin (Shanghai) 39:811–828

Galeron MA, Amiraux R, Charriere B, Radakovitch O and others (2015) Seasonal survey of the composition and degradation state of particulate organic matter in the Rhône River using lipid tracers. Biogeosciences 12: 1431–1446

Garel M, Bonin P, Martini S, Guasco S and others (2019) Pressure-retaining sampler and high-pressure systems to study deep-sea microbes under in situ conditions. Front Microbiol 10:453

Grant RJ, Betts BW (2004) Mineral and carbon usage of two synthetic pyrethroid degrading bacterial isolates. J Appl Microbiol 97:656–662

Guenet B, Danger M, Harrault L, Allard B and others (2014) Fast mineralization of land-born C in inland waters: first experimental evidence of aquatic priming effect. Hydrobiologia 721:35–44

Guenet B, Camino-Serrano M, Ciais P, Tifafi M, Maignan F, Soong JL, Janssens IA (2018) Impact of priming on global soil carbon stocks. Glob Chang Biol 24:1873–1883

Harwood JL, Russell NJ (1984) Major lipid types in plants and micro-organisms. In: Harwood JL, Russell NJ (eds) Lipids in plants and microbes. Springer, Dordrecht, p 7–34

Hedges JI (2002) Sedimentary organic matter preservation and atmospheric O_2 regulation. In: Gianguzza A, Pelizzetti E, Sammartano S (eds) Chemistry of marine water and sediments. Environmental Science. Springer, Berlin, p 105–123

Hedges JI, Keil RG (1995) Sedimentary organic matter preservation: an assessment and speculative synthesis. Mar Chem 49:81–115

Hedges JI, Keil RG, Benner R (1997) What happens to terrestrial organic matter in the ocean? Org Geochem 27: 195–212

Holloway PJ, Deas AHB (1973) Epoxyoctadecanoic acids in plant cutins and suberins. Phytochemistry 12: 1721–1735

Jackson CA, Couger MB, Prabhakaran M, Ramachandriya KD, Canaan P, Fathepure BZ (2017) Isolation and characterization of *Rhizobium* sp. strain YS-1r that degrades lignin in plant biomass. J Appl Microbiol 122:940–952

Jeffries TW (1991) Biodegradation of lignin-carbohydrate complexes. In: Ratledge C (eds) Physiology of biodegradative microorganisms. Springer, Dordrecht, p 163–176

Jones EBG, Irvine J (1971) Role of fungi in the deterioration of wood in the sea. Inst Wood Sci J 5:31–40

Karlsson ES, Charkin A, Dudarev O, Semiletov I and others (2011) Carbon isotopes and lipid biomarker investigation of sources, transport and degradation of terrestrial organic matter in the Buor-Khaya Bay, SE Laptev Sea. Biogeosciences 8:1865–1879

Kirchman DL (2002) The ecology of *Cytophaga-Flavobacteria* in aquatic environments. FEMS Microbiol Ecol 39:91–100

Kisand V, Cuadros R, Wikner J (2002) Phylogeny of culturable estuarine bacteria catabolizing riverine organic matter in the Northern Baltic Sea. Appl Environ Microbiol 68:379–388

Kolattukudy PE (1980) Biopolyester membranes of plants: cutin and suberin. Science 208:990–1000

Kuzyakov Y, Friedel JK, Stahr K (2000) Review of mechanisms and quantification of priming effects. Soil Biol Biochem 32:1485–1498

Langfelder P, Horvath S (2008) WGCNA: an R package for weighted correlation network analysis. BMC Bioinform 9:1–13

Lecornu J, Michel J (1986) L'étude d'impact de la protection contre les crues du Rhône des plaines de la région de Brangues. Société hydrotechnique de France. XIXe Journées de l'Hydraulique Paris, 9–11 sept.

Liu C, Cui Y, Li X, Yao M (2021) *microeco*: an R package for data mining in microbial community ecology. FEMS Microbiol Ecol 97:fiaa255

Lueders T, Manefield M, Friedrich MW (2004) Enhanced sensitivity of DNA- and rRNA-based stable isotope probing by fractionation and quantitative analysis of isopycnic centrifugation gradients. Environ Microbiol 6:73–78

Marchand D, Rontani JF (2001) Characterisation of photooxidation and autoxidation products of phytoplanktonic monounsaturated fatty acids in marine particulate matter and recent sediments. Org Geochem 32:287–304

Masai E, Katayama Y, Nishikawa S, Fukuda M (1999) Characterization of *Sphingomonas paucimobilis* SYK-6 genes involved in degradation of lignin-related compounds. J Ind Microbiol Biotechnol 23:364–373

McGrath CF, Moss CW, Burchard PR (1990) Effect of temperature shifts on gliding motility, adhesion, and fatty acid composition of *Cytophaga* sp. strain U67. J Bacteriol 172:1978–1982

McMurdie PJ, Holmes S (2013) phyloseq: an R package for reproducible interactive analysis and graphics of microbiome census data. PLOS ONE 8:e61217

Meyers PA, Eadie PJ (1993) Sources, degradation and recycling of organic matter associated with sinking particles in Lake Michigan. Org Geochem 20:47–56

Moss CW, Dees SB (1978) Cellular fatty acids of *Flavobacterium meningosepticum* and *Flavobacterium* species group Iib. J Clin Microbiol 8:772–774

Mouzouras R (1989) Soft rot decay of wood by marine microfungi. J Inst Wood Sci 11:193–201

Nedashkovskaya OI, Kim DB, Lysenko AM, Frolova GM, Mikhailov VV, Lee KH, Bae KS (2005) Description of *Aquimarina muelleri* gen. nov., sp. nov., and proposal of the reclassification of [Cytophaga] *latercula Lewin* 1969 as *Stanierella latercula* gen. nov., comb. nov. Int J Syst Evol Microbiol 55:225–229

Neufeld JD, Vohra J, Dumont MG, Lueders T, Manefield M, Friedrich MW, Murrell JC (2007) DNA stable-isotope probing. Nat Protoc 2:860–866

Newton RJ, Jones SE, Eiler A, McMahon KD, Bertilsson S (2011) A guide to the natural history of freshwater lake bacteria. Microbiol Mol Biol Rev 75:14–49

O'Sullivan LA, Weightman AJ, Fry JC (2002) New degenerate *Cytophaga-Flexibacter-Bacteroides*-specific 16S ribosomal DNA-targeted oligonucleotide probes reveal high bacterial diversity in river Taff epilithon. Appl Environ Microbiol 68:201–210

Obernosterer I, Catala P, Reinthaler T, Herndl GJ, Lebaron P (2005) Enhanced heterotrophic activity in the surface microlayer of the Mediterranean Sea. Aquat Microb Ecol 39:293–302

Otto A, Simoneit BRT, Rembe WC (2005) Conifer and angiosperm biomarkers in clay sediments and fossil plants from the Miocene Clarkia Formation, Idaho, USA. Org Geochem 36:907–922

Parada AE, Needham DM, Fuhrman JA (2016) Every base matters: assessing small subunit rRNA primers for marine microbiomes with mock communities, time series and global field samples. Environ Microbiol 18:1403–1414

Parnas H (1976) A theoretical explanation of the priming effect based on microbial growth with two limiting substrates. Soil Biol Biochem 8:139–144

Pointing SB, Hyde KD (2000) Lignocellulose-degrading marine fungi. Biofouling 15:221–229

Quast C, Pruesse E, Yilmaz P, Gerken J and others (2013) The SILVA ribosomal RNA gene database project: improved data processing and web-based tools. Nucleic Acids Res 41:D590–D596

Riemann L, Steward GF, Azam F (2000) Dynamics of bacterial community composition and activity during a mesocosm diatom bloom. Appl Environ Microbiol 66: 578–587

Rontani JF (2012) Photo-and free radical-mediated oxidation of lipid components during the senescence of phototrophic organisms. In: Nagata T (ed) Senescence. Intech, Rijeka, p 3–31

Rontani JF, Aubert C (2005) Characterization of isomeric allylic diols resulting from chlorophyll phytyl side chain photo- and autoxidation by electron ionization gas chromatography/mass spectrometry. Rapid Commun Mass Spectrom 19:637–646

Rontani JF, Belt ST (2020) Photo- and autoxidation of unsaturated algal lipids in the marine environment: an overview of processes, their potential tracers, and limitations. Org Geochem 139:103941

Rontani JF, Charrière B, Sempéré R, Doxaran D, Vaultier F, Vonk JE, Volkman JK (2014) Degradation of sterols and terrigenous organic matter in waters of the Mackenzie Shelf, Canadian Arctic. Org Geochem 75:61–73

Russa R, Urbanik-Sypniewska T, Lindström K, Mayer H (1995) Chemical characterization of two lipopolysaccharide species isolated from *Rhizobium loti* NZP2213. Arch Microbiol 163:345–351

Sanches JF, Guenet B, dos Anjos N, Marino C, de Assis Esteves F (2021) Exploring the drivers controlling the priming effect and its magnitude in aquatic systems. J Geophys Res Biogeosci 126(8):e2020JG006201

Schaich KM (2005) Lipid oxidation: theoretical aspects. In: Shahidi F(ed) Bailey's industrial oil and fat products. John Wiley & Sons, Chichester, p 269–355

Sonoki T, Iimura Y, Masai E, Kajita S, Katayama Y (2002) Specific degradation of β-aryl ether linkage in synthetic lignin (dehydrogenative polymerizate) by bacterial enzymes of *Sphingomonas paucimobilis* SYK-6 produced in recombinant *Escherichia coli.* J Wood Sci 48: 429–433

Steele JA, Countway PD, Xia L, Vigil PD and others (2011) Marine bacterial, archaeal and protistan association networks reveal ecological linkages. ISME J 5:1414–1425

Steen AD, Quigley LNM, Buchan A (2016) Evidence for the priming effect in a planktonic estuarine microbial community. Front Mar Sci 3:6

Sun MY, Shi W, Lee RF (2000) Lipid-degrading enzyme activities associated with distribution and degradation of

fatty acids in the mixing zone of Altamaha estuarine sediments. Org Geochem 31:889–902

Sun MY, He Y, Xiao Q, Ye R, Tian Y (2013) Isolation, characterization, and antimicrobial activity of endophytic bacteria from *Polygonum cuspidatum.* Afr J Microbiol Res 7: 1496–1504

Šuštar V, Zelko J, Lopalco P, Lobasso S and others (2012) Morphology, biophysical properties and protein-mediated fusion of archaeosomes. PLOS ONE 7:e39401

Teeling H, Fuchs BM, Becher D, Klockow C, Gardebrecht A, Bennke CM, Amann R (2012) Substrate-controlled succession of marine bacterioplankton populations induced by a phytoplankton bloom. Science 336:608–611

Treignier C, Derenne S, Saliot A (2006) Terrestrial and marine *n*-alcohol inputs and degradation processes relating to a sudden turbidity current in the Zaire canyon. Org Geochem 37:1170–1184

Triebl A, Wenk MR (2018) Analytical considerations of stable isotope labelling in lipidomics. Biomolecules 8:151

Vonk JE, Sanchez-Garcia L, Semiletov IP, Dudarev OV, Eglinton TI, Andersson A, Gustafsson Ö (2010) Molecular and radiocarbon constraints on sources and degradation of terrestrial organic carbon along the Kolyma paleoriver transect, East Siberian Sea. Biogeosciences 7:3153–3166

Ward ND, Bianchi TS, Sawakuchi HO, Gagne-Maynard W and others (2016) The reactivity of plant-derived organic matter and the potential importance of priming effects along the lower Amazon River. J Geophys Res Biogeosci 121:1522–1539

Ward ND, Bianchi TS, Medeiros PM, Seidel M, Richey JE, Keil RG, Sawakuchi HO (2017) Where carbon goes when water flows: carbon cycling across the aquatic continuum. Front Mar Sci 4:7

Ward ND, Sawakuchi HO, Richey JE, Keil RG, Bianchi TS (2019a) Enhanced aquatic respiration rates associated with mixing of clearwater tributary and turbid Amazon River waters. Front Earth Sci 7:101

Ward ND, Morrison E, Liu Y, Rivas-Ubach A, Osborne TZ, Ogram A, Bianchi TS (2019b) Marine microbial responses related to wetland carbon mobilization in the coastal zone. Limnol Oceanogr Lett 4:25–33

Ward ND, Megonigal JP, Bond-Lamberty B, Bailey VL, Butman D, Canuel EA, Windham-Myers L (2020) Representing the function and sensitivity of coastal interfaces in earth system models. Nat Commun 11:2458

Xu R, Zhang K, Liu P, Han H and others (2018) Lignin depolymerization and utilization by bacteria. Bioresour Technol 269:557–566

Yoon JH, Kang SJ, Yi HS, Oh TK, Ryu CM (2010) *Rhizobium soli* sp. nov., isolated from soil. Int J Syst Evol Microbiol 60:1387–1393

Zamora L, Vela AI, Sánchez-Porro C, Palacios MA and others (2013) Characterization of flavobacteria possibly associated with fish and fish farm environment. Description of three novel *Flavobacterium* species: *Flavobacterium collinsii* sp. nov., *Flavobacterium branchiarum* sp. nov., and *Flavobacterium branchiicola* sp. nov. Aquaculture 416–417:346–353

Editorial responsibility: Ilana Berman-Frank, Haifa, Israel
Reviewed by: A. Sichert and 1 anonymous referee

Submitted: September 21, 2022
Accepted: May 19, 2023
Proofs received from author(s): July 27, 2023